Scientific Research Publishing

Modern Research in Catalysis, 2021, 10, 56-72
https://www.scirp.org/journal/mrc
ISSN Online: 2168-4499
ISSN Print: 2168-4480

Monolithic Mesh-Type Fe-Pd/γ-Al_2O_3/Al Bifunctional Catalysts for Electro-Fenton Degradation of Rhodamine B

Qianwen Shao, Guiru Zhang, Linhui Lu, Qi Zhang*

Department of Chemical Engineering, East China University of Science and Technology, Shanghai, China
Email: *zhangqi@ecust.edu.cn

How to cite this paper: Shao, Q.W., Zhang, G.R., Lu, L.H. and Zhang, Q. (2021) Monolithic Mesh-Type Fe-Pd/γ-Al_2O_3/Al Bifunctional Catalysts for Electro-Fenton Degradation of Rhodamine B. *Modern Research in Catalysis*, **10**, 56-72.
https://doi.org/10.4236/mrc.2021.102004

Received: April 1, 2021
Accepted: April 23, 2021
Published: April 26, 2021

Abstract

A novel Fe-Pd bifunctional catalyst supported on mesh-type γ-Al_2O_3/Al was prepared and applied in the degradation of Rhodamine B (RhB). The monolithic mesh-type Fe-Pd/γ-Al_2O_3/Al bifunctional catalyst could be separated from the solution directly and could synthesize H_2O_2 in situ. The characterization results showed that Fe could improve the dispersion of Pd^0, and the electronic interactions between Pd and Fe could increase the Pd^0 contents on the catalyst, which increased the productivity of H_2O_2. Furthermore, DFT calculations proved that the addition of Fe could inhibit the dissociation of O_2 and promote the nondissociative hydrogenation of O_2 on the surface of Fe-Pd/γ-Al_2O_3/Al, which resulted in the increasement of H_2O_2 selectivity. Finally, the in-situ synthesized H_2O_2 by Pd was furtherly decomposed in situ by Fe to generate •OH radicals to degrade organic pollutants. Therefore, Fe-Pd/γ-Al_2O_3/Al catalysts exhibited excellent catalytic activity in the in-situ synthesis of H_2O_2 and the degradation of RhB due to the synergistic effects between Pd and Fe on the catalyst. It provided a new idea for the design of bifunctional electro-Fenton catalysts. Ten cycles of experiments showed that the catalytic activity of Fe-Pd/γ-Al_2O_3/Al catalyst could be maintained for a long time.

Keywords

Rhodamine B, Fe-Pd/γ-Al_2O_3/Al Catalyst, Electro-Fenton, Hydrogen Peroxide, Synergistic Effects

1. Introduction

Advanced oxidation technology has been widely used in the degradation of organic pollutants in wastewater and the remediation of groundwater based on the

generation of strong oxidizing •OH radicals [1] [2]. Among the AOPs, Fenton oxidation is particularly effective for the treatment of organic wastewater that is difficult to degrade by biological or general chemical oxidation. However, in the traditional Fenton oxidation process, a large amount of iron sludge is produced, which causes secondary pollution [3], and the addition of hydrogen peroxide is needed, which is dangerous and expensive for the production, transportation and storage.

Heterogeneous Fenton oxidation can overcome the shortcomings of iron sludge, in which, the active components Fe or Cu are fixed in the structure of catalysts [4] [5]. On the other side, a novel electro-Fenton process that can continuously synthesize H_2O_2 in situ has attracted great interests [6] [7]. By combining heterogeneous Fenton reaction with electro-Fenton reaction, the H_2O_2 synthesized in situ can be simultaneously decomposed by Fe on the catalysts into •OH radicals, which finally degrading or even mineralizing organic contaminants.

Table 1 summarized the application of different heterogeneous electro-Fenton catalysts in organic pollutants degradation. It shows that there are two ways to synthesize H_2O_2 in situ: 1) H_2O_2 is synthesized from H_2 and O_2 under the catalysis of Pd; 2) H_2O_2 is synthesized from two-electron reduction of O_2 at the cathode. Compared to the continuous pumping of O_2 to the cathode, the use of electro-generated H_2 and O_2 was a safer and more controllable way to continuously synthesize H_2O_2 [8].

It was also noted that all catalysts were particles or powders. Although it was convenient for research, it was difficult to recycle in industrial applications. Therefore, how to structure the catalysts is a big problem for the heterogeneous electro-Fenton degradation of organic pollutants.

In addition, though H_2O_2 can be synthesized by Pd catalysts, the selectivity is

Table 1. List of heterogeneous electro-Fenton catalysts for organic pollutants degradation.

Catalysts	Type	Operation Conditions	DyeRemoval/%	H_2O_2 Formation	Author and Reference
0.5 g Pd/C (5 wt% Pd)	particles	200 mL 10 mg/L RhB, 50 mA, 1 mM Fe^{2+}	30 min, 84.4%	$H_2 + O_2 \rightarrow H_2O_2$	Yuan, S *et al.* [7]
0.2 g Pd/MNPs (5 wt% Pd)	nanoparticles	200 mL 20 mg/L phenol, 50 mA, pH 3	60 min, 98%	$H_2 + O_2 \rightarrow H_2O_2$	Luo, M *et al.* [9]
0.05 g Pd@Fe_3O_4	nanoparticles	500 mL 2 mg/L IBP, 30 V, pH 5.2, ultrasound	60 min, 97%	$H_2 + O_2 \rightarrow H_2O_2$	Thokchom, B *et al.* [10]
0.2 g Cu/C (2 wt% Cu)	particles	200 mL 2 mg/L phenol, 50 mA, 10 mg/L Fe^{2+}, pH 3	180 min, 90%	$H_2 + O_2 \rightarrow H_2O_2$	Xu, X *et al.* [11]
11.25 mg Fe-SBA-15	powder	750 mL 10 mg/L RhB, 8 V, pH 2, O_2 supplied	180 min, 97.7%	$O_2 + 2H^+ + 2e^- \rightarrow H_2O_2$	Jinisha, R *et al.* [12]
0.1 g $FeVO_4/CeO_2$	nanocomposite	100 mL 30 mg/L MO, 200 mA, pH 3, O_2 supplied	60 min, 96.31%	$O_2 + 2H^+ + 2e^- \rightarrow H_2O_2$	Setayesh, S. R *et al.* [13]

limited. In the process of in-situ synthesis of H_2O_2, the nondissociative hydrogenation of O_2 on Pd surface is the main side reaction [14]. Many researchers were interested in adding a second metal to Pd catalysts to improve the selectivity of H_2O_2 [15]-[20]. Suli Wang *et al*. demonstrated that the addition of Zn could modify the geometric structure of Pd catalysts, and the electronic interactions between Zn and Pd could improve the selectivity of H_2O_2 [15]. Jun Li *et al*. compared the in-situ synthesis of H_2O_2 from H_2 and O_2 on the surface of Au-Pd(111) and Pd(111), and found that on the Au-Pd(111) surface, the main reactions for H_2O_2 synthesis exceeded all side reactions due to the co-adsorption of H atoms [16]. Doudou Ding *et al*. reported that Sb could inhibit the oxidation of Pd, and increase the proportion of Pd monomer sites that were beneficial for H_2O_2 formation [17]. Therefore, how to prepare an easy-to-recycle structured electro-Fenton catalyst with high H_2O_2 selectivity and removal efficiency should be an important research item.

In this research, a novel monolithic mesh-type Fe-Pd/γ-Al_2O_3/Al bifunctional catalyst was synthesized and applied in electro-Fenton degradation of Rhodamine B (RhB). Firstly, the geometric change of catalysts caused by Fe addition was studied by SEM, BET and XRD. Secondly, the synergistic effects between Pd and Fe on the in-situ synthesis of H_2O_2 and the decomposition of H_2O_2 to produce •OH radicals in situ were investigated by experiments and calculations. Based on the above research, a possible reaction mechanism for organic pollutants degradation by Fe-Pd/γ-Al_2O_3/Al was proposed. Finally, the durability of Fe-Pd/γ-Al_2O_3/Al catalyst was evaluated by ten cycles of experiments.

2. Experimental

2.1. Catalyst Preparation

The γ-Al_2O_3/Al support was prepared by anodizing technology. First, the commercial Al mesh was washed with 10 wt% NaOH solution for 4 min, and washed with 10 wt% HNO_3 solution for 2 min, and then washed with deionized water. Second, the washed Al mesh was put into a 0.4 mol/L oxalic acid solution at 25˚C and anodized for 10 hours, the current density was set to 25 A/m^2. The anodized Al mesh was calcined at 350˚C for 1 h to form anodized aluminum oxide (AAO). Third, the AAO was hydrated in 80˚C deionized water for 1 h. Finally, the hydrated AAO was dried at room temperature followed by calcining at 500˚C for 4 h to form γ-Al_2O_3/Al support.

A series of Fe-Pd/γ-Al_2O_3/Al bimetallic catalysts with different Fe contents were synthesized via successive impregnation methods. First the γ-Al_2O_3/Al supports were impregnated in 0.05 mol/L ferric nitrate solution for different time, then dried and calcined at 500˚C for 4 h. Second, the prepared Fe_x/γ-Al_2O_3/Al catalysts were impregnated in 0.08 g/L palladium nitrate solution for 12 h, then dried and calcined at 550˚C for 4 h. Finally, the calcined catalysts were reduced in 0.05 mol/L sodium borohydride solution for 1 h. The resulting catalysts were denoted as Fe_x-Pd/γ-Al_2O_3/Al, where x is the contents of Fe.

2.2. Catalyst Characterization

The specific surface areas and pore size distribution of the support and different catalysts were measured by N_2 adsorption and desorption method through ASAP 2020-M instrument (Micromeritics, USA). The actual contents of Pd and Fe on the catalysts were measured by inductively coupled plasma atomic emission spectrometry (ICP-AES, Varian, USA). The phases of crystals on the catalysts were detected by X-ray diffraction (XRD) patterns using D/max 2250 VB/PC diffractometer (Rigaku, Japan). Scanning electron microscopy (SEM, JEM-6360LV, JEOL) was used to observe the cross-sectional morphology and the surface structure of catalysts. The chemical states of elements on different catalysts were elucidated by X-ray photoelectron spectroscopy (XPS) using ESCALAB 250Xi electron spectrometer (Thermo Scientific Corporation, USA). The calibration of binding energies was referred to C 1s peaks at 284.8 eV.

2.3. Catalyst Activity Test

Batch electrolytic experiments were carried out in a glass beaker with a capacity of 250 mL. As shown in Figure 1, two flakes of Pt (1 × 1 cm) were used as the cathode and anode. For each test, 250 mL solution containing 10 mg/L RhB and 0.1 M Na_2SO_4 were added into the glass beaker, 0.2 g (2.5 × 3 cm) mesh-type catalyst was suspended in the solution. The initial pH of the solution was adjusted to 2 by the addition of 0.1 M H_2SO_4 using a pH-meter. The beaker was put in a magnetic stirring water bath to maintain a certain temperature and stirring rate. A constant current was provided by a DC power supply (MN-3205D, 32V/5A). During the electrolysis, about 2 mL of electrolysed RhB solution was taken out from the beaker at regular time intervals, and the residual RhB concentration was measured by the ultraviolet-visible spectrophotometer (UV752, Shanghai YoKe Instrument Co., LTD) at 554 nm.

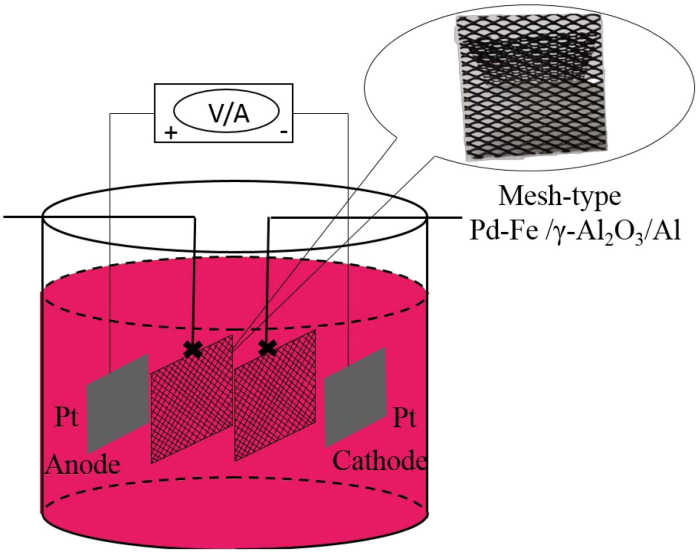

Figure 1. Schematic diagram of electro-Fenton degrading RhB.

2.4. DFT Method

DFT calculations were carried out by Vienna ab initio simulation package (VASP) [21]. Perdew-Burke-Ernzerhof (PBE) was used for self-consistent description of exchange-correlation functions [22]. The energy cutoff of plane wave expansion was set to 500 eV. The surface Brillouin zone was sampled with a 3 × 3 × 1 Monkhorst-Pack k-points grid mesh for all slabs [23]. The interaction between adjacent slabs was eliminated by setting a 15 Å vacuum space in the vertical direction. The top layer of atoms and the adsorbates were relaxed, while the two layers of atoms in the bottom were fixed in corresponding positions. The transition states were searched by climbing image nudged elastic band (cNEB) method [24] and vibration frequency analysis.

The adsorption energy (E_{ads}) of the adsorbate on slab model surface was defined as

$$E_{ads} = E_{ads/sub} - E_{ads} - E_{sub} \quad (1)$$

where $E_{ads/sub}$, E_{ads}, and E_{sub} were the energies of adsorbed species stably adsorbed on the surface, adsorbed species, and a clean surface, respectively.

The reaction barrier (E_a) was defined as

$$E_a = E_{TS} - E_{IS} \quad (2)$$

where E_{TS} and E_{IS} were the energies of transition states and initial states, respectively.

3. Results and Discussion

3.1. Characterization of Catalysts

Figure 2(a) shows the well-dense and ordered pore structure on the surface of AAO/Al. After hot water treatment and calcination, the surface of γ-Al_2O_3/Al became rough and formed a honeycomb porous structure (**Figure 2(b)**). For Pd/γ-Al_2O_3/Al (**Figure 2(c)**), there were obvious Pd particle aggregates covering the surface of γ-Al_2O_3/Al support. As for Fe-Pd/γ-Al_2O_3/Al catalyst (**Figure 2(d)**), there were no obvious Pd particles on the surface, indicating that adding Fe could reduce the particle size and improve the dispersion of Pd.

Table 2 shows textural properties of the support and catalysts. It was found that the specific surface area of AAO/Al was only 8 m^2/g and the average pore diameter was 12.6 nm. After hot water treatment and calcination, the specific surface area of γ-Al_2O_3/Al was increased to 127 m^2/g and the average pore diameter was decreased to 5.19 nm. It confirmed that the support had a high specific surface area. After loading Pd or Fe on the support, both the specific surface areas and pore volume reduced due to pore blockage. However, compared to Pd/γ-Al_2O_3/Al, the S_{BET} and V_p of Fe-Pd/γ-Al_2O_3/Alslightly increased, this change could be explained as the addition of Fe promoted the dispersion of Pd.

The crystal phases of the support and different catalysts were detected by XRD measurements. From **Figure 3**, it can be seen that the characteristic diffraction peaks of γ-Al_2O_3/Al at 2θ = 45.8˚ and 67.0˚ were present in all catalysts. For

Pd/γ-Al_2O_3/Al catalyst, there was an additional diffraction peak at 40.1˚ corresponding to (111) crystal plane of metallic Pd^0, which was benefit for H_2O_2 generation [25]. Meanwhile, it can be found that different from Pd/γ-Al_2O_3/Al, the intensity of the characteristic diffraction peak for Pd (111) in Fe-Pd/γ-Al_2O_3/Algets weak, which can be attributed to the interaction between Pd and Fe, that is, doping with Fe can improve the dispersion of Pd [17] [26]. However, no diffraction peaks of iron oxide could be detected in the patterns of Fe-Pd/γ-Al_2O_3/Al, it

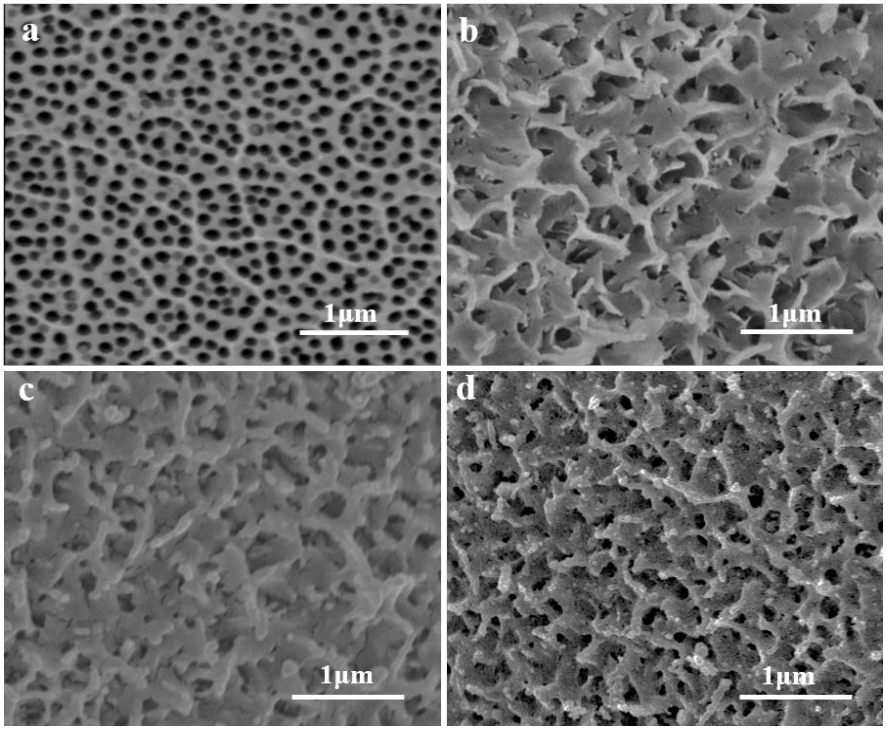

Figure 2. The SEM images of AAO/Al (a); γ-Al_2O_3/Al (b); Pd/γ-Al_2O_3/Al (c) and Fe-Pd/γ-Al_2O_3/Al (d).

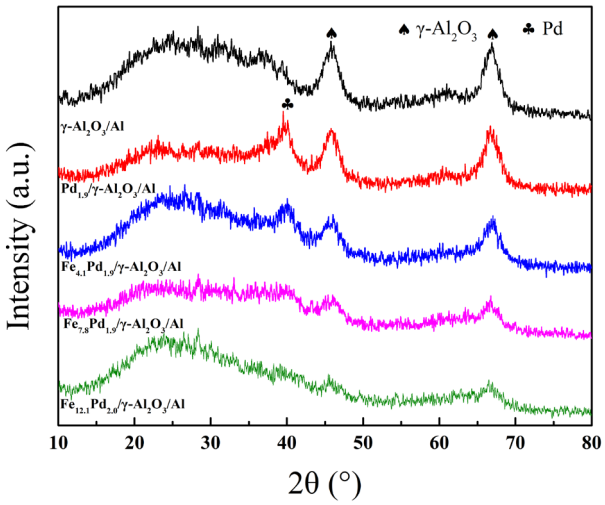

Figure 3. XRD patterns of support γ-Al_2O_3/Al and different catalysts.

Table 2. Chemical compositions and textural properties of all catalysts.

Catalysts	Loading (wt%)		S_{BET} (m^2/g)	V_p (mL/g)	D_p (nm)
	Fe	Pd			
AAO/Al			8	0.05	12.60
γ-Al_2O_3/Al	-	-	127	0.29	5.19
$Fe_{7.9}$/γ-Al_2O_3/Al	7.9	-	100	0.25	9.15
$Pd_{1.9}$/γ-Al_2O_3/Al	-	1.9	72	0.14	8.99
$Fe_{4.1}Pd_{1.9}$/γ-Al_2O_3/Al	4.1	1.9	86	0.21	7.05
$Fe_{7.8}Pd_{1.9}$/γ-Al_2O_3/Al	7.8	1.9	120	0.22	6.54
$Fe_{12.1}Pd_{2.0}$/γ-Al_2O_3/Al	12.1	2.0	112	0.21	7.20

could be explained that the particle size of iron oxide was very small or amorphous [27].

The chemical states of Pd and Fe on different catalysts were identified by XPS. **Figure 4** shows the Fe 2p and Pd 3d XPS spectra of different catalysts. From **Figure 4(a)**, it can be seen that the XPS spectra of Fe 2p can be deconvoluted into Fe^{2+} (red line) and Fe^{3+} (blue line) peaks, and compared with Fe/γ-Al_2O_3/Al, the binding energy of Fe 2p on Fe-Pd/γ-Al_2O_3/Al catalysts shifts toward high values. At the same time, the XPS spectra of Pd 3d in **Figure 4(b)** can also be divided into Pd^0 (red line) and Pd^{2+} (blue line) peaks. Different from the chemical shift of Fe 2p, the binding energy of Pd 3d on Fe-Pd/γ-Al_2O_3/Al catalysts shifted toward low values compared with Pd/γ-Al_2O_3/Al. The differences in chemical shift of Pd and Fe were due to the transfer of electrons from Fe to Pd, which was consistent with the higher electronegativity of Pd (2.2) than that of Fe (1.8) [28] [29]. To visually observe the Pd and Fe contents on different catalysts, **Table 3** summarized the relative contents of Pd and Fe on different catalysts, which were calculated from the curve fitting in XPS spectra. The data show that $Fe_{7.8}Pd_{1.9}$/γ-Al_2O_3/Al catalyst has the highest Pd^0 contents, it confirms that there is an optimal ratio between Pd and Fe.

3.2. Application of Fe-Pd/γ-Al_2O_3/Al Catalysts in Electro-Fenton Reaction

The activity of catalysts was evaluated by RhB degradation. For comparison, Fe/γ-Al_2O_3/Al catalyst was used to degrade RhB by Fenton-like reaction without electricity. As shown in **Figure 5(a)**, H_2O_2 plays an important role in the Fenton-like system. Without H_2O_2, RhB would not be degraded by Fe/γ-Al_2O_3/Al catalyst. With the increase of H_2O_2 concentrations, the degradation rate of RhB was also increased, and when the concentration of H_2O_2 reached 1200 ppm, 80% of RhB was degraded within 2 hours. However, in the electro-Fenton system, H_2O_2 was not needed. **Figure 5(b)** discussed the effects of electric currents on the degradation of RhB. The result showed that the degradation rate of RhB increased with the electric currents increasing. When the electric current was 50 mA, 98% of RhB was degraded within 2 hours. **Figure 5(c)** exhibited that as the

Table 3. Fe and Pd concentrations of different catalysts.

Catalysts	Pd 3d		Fe 2p	
	Pd^0 (%)	Pd^{2+} (%)	Fe^{2+} (%)	Fe^{3+} (%)
Fe/γ-Al_2O_3/Al	-	-	49.6	50.4
Pd/γ-Al_2O_3/Al	49.0	51.0	-	-
$Fe_{4.1}Pd_{1.9}$/γ-Al_2O_3/Al	52.9	47.1	52.4	47.6
$Fe_{7.8}Pd_{1.9}$/γ-Al_2O_3/Al	61.6	38.4	56.8	43.2
$Fe_{12.1}Pd_{2.0}$/γ-Al_2O_3/Al	53.8	46.2	50.2	49.8

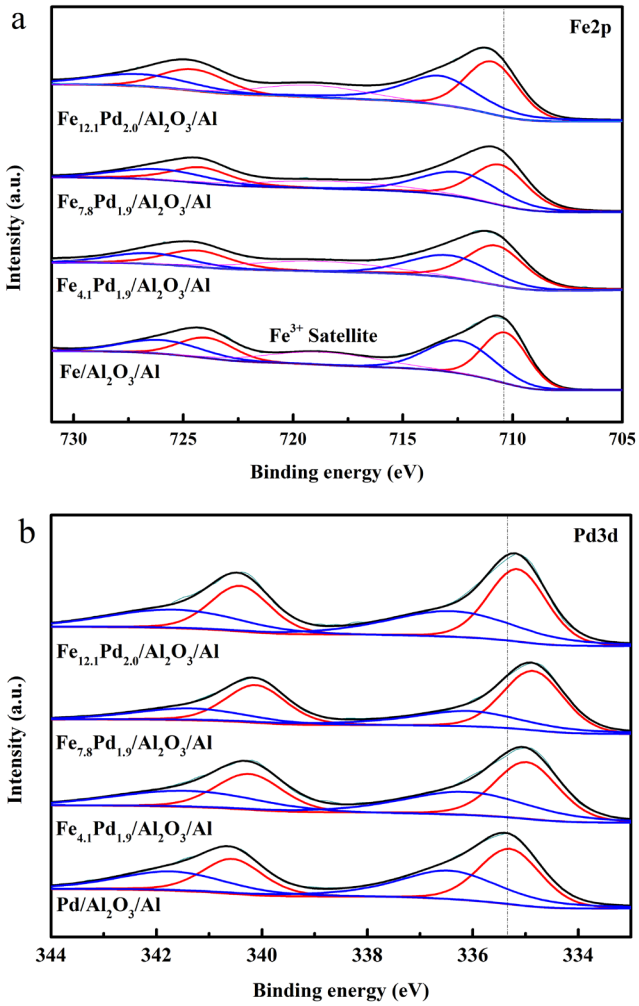

Figure 4. XPS spectra of Fe 2p (a) and Pd 3d (b) for different catalysts.

pH value decreased, RhB degradation increased significantly, and when the pH value was 2, 96% of RhB could be degraded within 1 hours.

In the meantime, in order to verify the synergistic effects between Pd and Fe, different catalysts that were Pd/γ-Al_2O_3/Al, Fe/γ-Al_2O_3/Al, the mixture of Pd/γ-Al_2O_3/Al and Fe/γ-Al_2O_3/Al, and Fe-Pd/γ-Al_2O_3/Al were applied in electro-Fenton degradation of RhB. **Figure 5(d)** shows that the degradation rate of

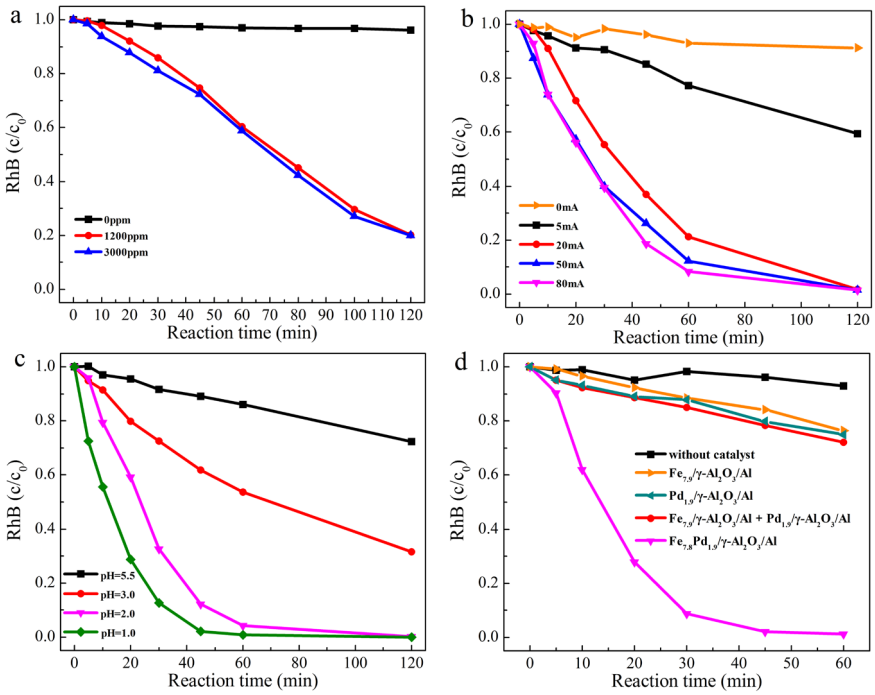

Figure 5. Degradation of RhB under different conditions. (a) Fenton-like reaction without electricity under different H_2O_2 concentration; (b) electro-Fenton reaction under different electric currents; (c) electro-Fenton reaction under different pH; (d) electro-Fenton degradation RhB over different catalysts. Unless otherwise specified, the reactions were carried out under the conditions of 250 mL of 10 mg/L initial RhB, pH 2, 50 mA, 0.8 g/L catalyst, 25˚C, 300 rpm.

RhB on monometallic Pd/γ-Al_2O_3/Al and Fe/γ-Al_2O_3/Al catalysts is very low, which indicates that the catalytic activity of monometallic catalysts is very small. In addition, the mixture of Fe/γ-Al_2O_3/Al and Pd/γ-Al_2O_3/Al was used, and the total amounts were equal to Fe-Pd/γ-Al_2O_3/Al. The results show that the degradation rate of RhB by Pd/γ-Al_2O_3/Al and Fe/γ-Al_2O_3/Al mixture is much lower than that by Fe-Pd/γ-Al_2O_3/Al. It indicated that the synergistic effects between Pd and Fe really existed.

To verify H_2O_2 was synthesized in situ in this electro-Fenton system, the concentration of H_2O_2 synthesized in water was measured at 400 nm after coloring with potassium titanium oxalate [30]. **Figure 6(a)** shows that without catalyst, almost no H_2O_2 is formed, indicating that the amount of H_2O_2 synthesized by O_2 reduction in this system is very small. Interestingly, the concentration of H_2O_2 synthesized by the mixture of Fe/γ-Al_2O_3/Al and Pd/γ-Al_2O_3/Al increased with time, while the concentration of H_2O_2 synthesized by Fe-Pd/γ-Al_2O_3/Al had a decreasing process. It was because the H_2O_2 synthesized in situ by Fe-Pd/γ-Al_2O_3/Al could be immediately decomposed by Fe which was on the catalyst. In addition, the concentration of H_2O_2 synthesized by $Fe_{7.8}Pd_{1.9}$/γ-Al_2O_3/Al was higher than $Fe_{4.1}Pd_{1.9}$/γ-Al_2O_3/Al and $Fe_{12.1}Pd_{2.0}$/γ-Al_2O_3/Al, which was due to the highest Pd^0 contents on $Fe_{7.8}Pd_{1.9}$/γ-Al_2O_3/Al catalyst.

In order to test the generation of •OH radicals, electro-Fenton degradation of

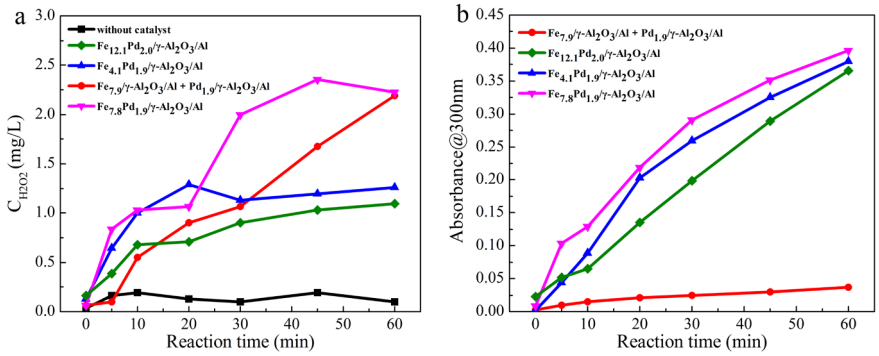

Figure 6. In situ generation of H_2O_2 (a), changes in absorbance at 300 nm (b) over different catalysts. The reactions were carried out under the conditions of 250 mL solution, pH 2, 50 mA, 0.8 g/L catalyst, 25˚C, 300 rpm.

100 mg/L of benzoic acid was carried out. Since benzoic acid could be decomposed by •OH radicals to produce salicylic acid, the generation of salicylic acid could reflect the generation of •OH radicals. The formation of salicylic acid could be measured at 300 nm absorbance [31]. **Figure 6(b)** shows that the increase rate of •OH radicals generated by Fe-Pd/γ-Al_2O_3/Al is far higher than that of by the mixture of Fe/γ-Al_2O_3/Al and Pd/γ-Al_2O_3/Al, which corresponds to the change in H_2O_2 concentration and the difference in catalytic activity. Similarly, the concentration of •OH radicals generated by $Fe_{7.8}Pd_{1.9}/\gamma$-Al_2O_3/Al was higher than $Fe_{4.1}Pd_{1.9}/\gamma$-Al_2O_3/Al and $Fe_{12.1}Pd_{2.0}/\gamma$-Al_2O_3/Al, which was due to the high H_2O_2 concentration generated by $Fe_{7.8}Pd_{1.9}/\gamma$-Al_2O_3/Al.

The above experimental results indicated that by combining Pd in-situ synthesis of H_2O_2 and Fe decomposition of H_2O_2 to generate •OH radicals, the organic pollutants in the solution could be effectively removed.

DFT calculations were further used to discuss the effects of Fe on the selectivity of H_2O_2 synthesized by Pd. As mentioned above, the selectivity of H_2O_2 depended on the competition between the nondissociative hydrogenation reaction and the dissociation reaction of O-O bond species on the catalyst surface [32] [33]. The O_2 nondissociative hydrogenation to OOH intermediate was generally considered the rate-determining step for H_2O_2 synthesis [34] [35]. First, the dissociation of O_2 on the surface of Fe-Pd/γ-Al_2O_3/Al and Pd/γ-Al_2O_3/Al was investigated. From **Figure 7(a)**, it can be seen that the reaction barrier of O_2 dissociation on the Fe-Pd/γ-Al_2O_3/Al surface is 1.47 eV, which is much higher than 0.66 eV on the surface of Pd/γ-Al_2O_3/Al. It indicated that the O_2 dissociation on the Fe-Pd/γ-Al_2O_3/Al surface was relatively difficult. After that, we calculated the nondissociative hydrogenation energy barrier of O_2 on the surface of Fe-Pd/γ-Al_2O_3/Al and Pd/γ-Al_2O_3/Al. **Figure 7(b)** shows that the reaction barrier of O_2nondissociative hydrogenation on Fe-Pd/γ-Al_2O_3/Al surface is 0.44 eV, lower than 0.56 eV on the surface of Pd/γ-Al_2O_3/Al. It meant that the nondissociative hydrogenation reaction of O_2 was more likely to occur on the Fe-Pd/γ-Al_2O_3/Al surface than the dissociation reaction. Based on the DFT calculation results, we can infer that adding Fe can improve the selectivity of H_2O_2.

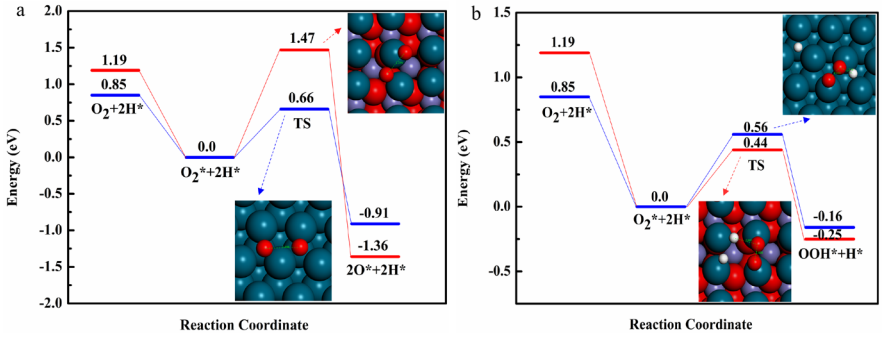

Figure 7. Energy diagram for (a) the dissociation of O_2 and (b) the non-dissociative hydrogenation of O_2 on the surface of Fe-Pd/γ-Al_2O_3/Al (red line) and Pd/γ-Al_2O_3/Al (blue line).

3.3. Possible Mechanisms of Fe-Pd/γ-Al_2O_3/Al Electrocatalytic System

Radicals scavenging experiments were carried out to determine the contribution of •OH radicals to RhB degradation. Isopropanol was widely used to scavenge •OH radicals. From **Figure 8**, it can be seen that after adding 100 mM isopropanol to the reaction system, the RhB degradation rate is remarkably inhibited, which validated that •OH radicals were the main active oxygen species that degrade RhB in the electro-Fenton system.

Therefore, according to the above experimental results, a possible reaction mechanism of Fe-Pd/γ-Al_2O_3/Al catalysts for organic pollutants degradation was proposed, as shown in **Figure 9**. First, H_2 and O_2 were produced by the electrolysis of water, the produced H_2 and O_2 adsorbed on Fe-Pd/γ-Al_2O_3/Al surface, then H_2O_2 was synthesized under the catalysis of Pd. In H_2O_2 synthesis step, Fe could improve the selectivity of H_2O_2, due to the addition of Fe could increase the contents and dispersion of Pd^0, also inhibit the dissociation of O_2 and promote the nondissociative hydrogenation of O_2. Finally, the in-situ synthesized H_2O_2 was decomposed by $\equiv Fe^{2+}$ on the catalyst to produce •OH radicals, which ultimately degraded organic pollutants into CO_2 and other by-products. At the same time, comparing the content of $\equiv Fe^{2+}$ and $\equiv Fe^{3+}$ on Fe-Pd/γ-Al_2O_3/Al catalysts before and after reaction (56.8% and 43.1%, 55.7% and 44.3%, respectively), it was found that there was no obvious change. It confirmed that the electronic interactions between Pd and Fe could promote the circulation of $\equiv Fe^{2+}/\equiv Fe^{3+}$ on the catalyst.

3.4. Durability of Fe-Pd/γ-Al_2O_3/Al Catalyst

The reusability of Fe-Pd/γ-Al_2O_3/Al catalyst was tested through ten RhB degradation experiments. After each cycle experiment, fresh RhB was added into the beaker to make the initial concentration reach 10 mg/L. **Figure 10** shows that the degradation rate of RhB can be maintained above 90% in each cycle experiment, indicating that the catalyst can be reused for a long time.

The concentration of leached Fe ions during the electrolysis was measured,

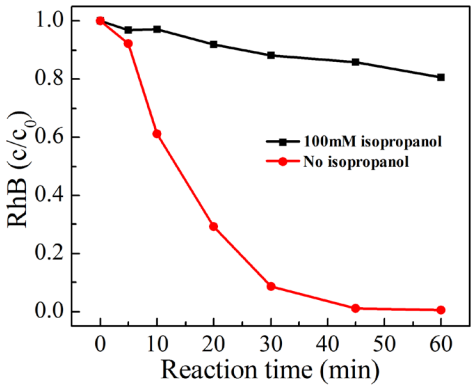

Figure 8. Effects of radical scavenging agent on RhB degradation. Unless otherwise specified, the reactions were carried out under the conditions of 250 mL of 10 mg/L initial RhB, pH 2, 50 mA, 0.8 g/L catalyst, 25˚C, 300 rpm.

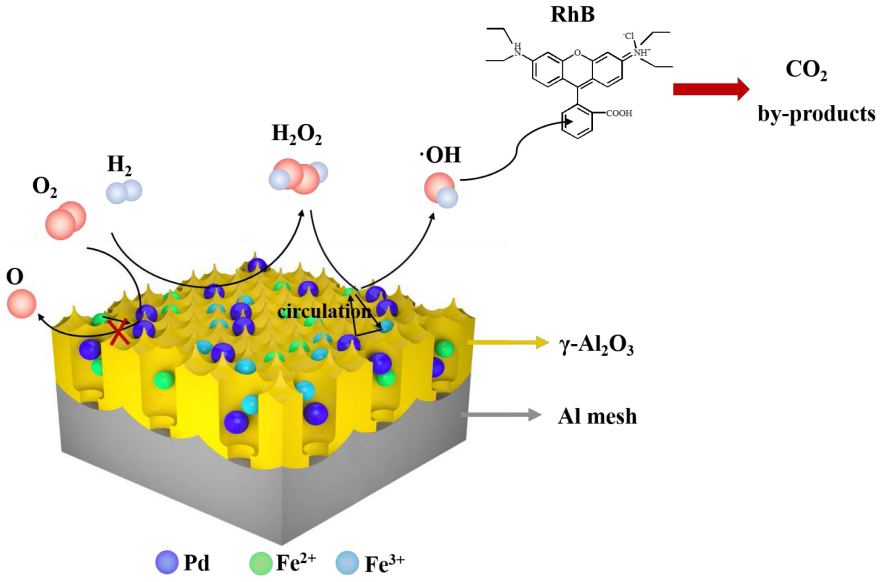

Figure 9. Proposed mechanism of Fe-Pd/γ-Al_2O_3/Al electrocatalytic system to degrade organic pollutants.

and the results were shown in **Figure 11**. The concentration of leached Fe^{2+} was measured at 510 nm using the modified 1,10-phenanthroline method, and the concentration of leached Fe^{3+} was measured at 525 nm by generating ferric-salicylic acid complexes [36]. It can be seen that the concentration of leached Fe^{3+} increases with time and reaches a plateau value of about 1.6 mg/L after 60min, while the concentration of leached Fe^{2+} increases with time, reaches the maximum at 90min, and then decreases with time. The fluctuation was mainly due to the homogeneous Fenton oxidation. Generally, in the process of homogeneous electro-Fenton reaction, the added or leached Fe^{2+} concentration was greater than 10 mg/L [9]. But the lower concentration of leached Fe^{2+} and Fe^{3+} in this electro-Fenton system indicated that the degradation of RhB by

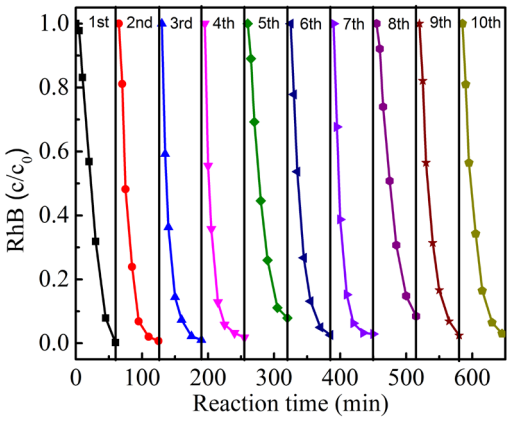

Figure 10. Durability of Fe-Pd/γ-Al_2O_3/Al. Unless otherwise specified, the reactions were carried out under the conditions of 250 mL of 10 mg/L initial RhB, pH 2, 50 mA, 0.8 g/L catalyst, 25˚C, 300 rpm.

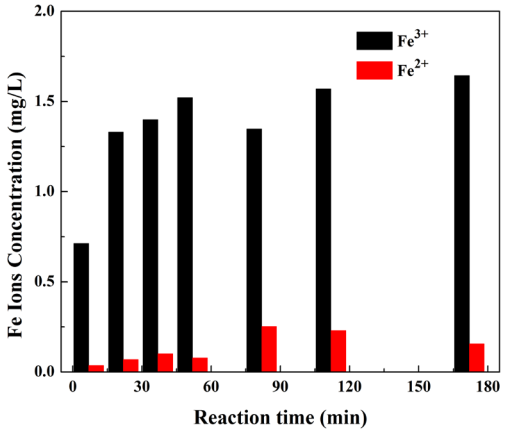

Figure 11. Accumulation of leached Fe^{2+} and Fe^{3+} ions during electrolysis. Unless otherwise specified, the reactions were carried out under the conditions of 250 mL of 10 mg/L initial RhB, pH 2, 50 mA, 0.8 g/L catalyst, 25˚C, 300 rpm.

Fe-Pd/γ-Al_2O_3/Al was mainly due to the Fe ions on the catalyst.

4. Conclusion

A novel monolithic mesh-type Fe-Pd/γ-Al_2O_3/Al bifunctional catalyst was synthesized and applied in electro-Fenton degradation of RhB. The Fe-Pd/γ-Al_2O_3/Al catalyst showed the high catalytic activity in the in-situ synthesis of H_2O_2 and the degradation of RhB. The addition of Fe could promote the dispersion of Pd, and due to the electronic interactions between Pd and Fe, electrons were transferred from Fe to Pd. Therefore, the dispersion and content of Pd^0 on the Fe-Pd/γ-Al_2O_3/Al catalyst increased, which could provide more active sites for the synthesis of H_2O_2. The addition of Fe could increase the reaction barrier of O_2 dissociation, and reduce the reaction barrier of O_2 nondissociative hydrogenation

on the surface of Pd, which increased the selectivity of H_2O_2. Subsequently, the H_2O_2 synthesized in situ was immediately decomposed by Fe on the Fe-Pd/γ-Al_2O_3/Al catalyst to generate •OH radicals, which ultimately degraded RhB. For ten cycles of RhB degradation experiments, Fe-Pd/γ-Al_2O_3/Al catalyst showed good catalytic activity. However, the productivity of H_2O_2 and the durability of the catalyst needed further study.

Acknowledgements

This work was financially supported by the National Key Research and Development Project (Grant NO. 2018YFB0105603) and the Shandong Greenwater Environmental Protection Technology Co., Ltd.

Conflicts of Interest

The authors declare no conflicts of interest regarding the publication of this paper.

References

[1] Fernández-castro, P., Vallejo, M., Fresnedo, M., Román, S. and Ortiz, I. (2015) Insight on the Fundamentals of Advanced Oxidation Processes. Role and Review of the Determination Methods of Reactive Oxygen Species. *Journal of Chemical Technology and Biotechnology*, **90**, 796-820. https://doi.org/10.1002/jctb.4634

[2] Brillas, E., Sirés, I. and Oturan, M.A. (2009) Electro-Fenton Process and Related Electrochemical Technologies Based on Fenton's Reaction Chemistry. *Chemical Reviews*, **109**, 6570-6631. https://doi.org/10.1021/cr900136g

[3] Guo, P. and Jin, X. (2018) The Catalytic Effect of Nano-Fe_3O_4 on RhB Decolorization by CGDE Process. *Catalysis Communications*, **106**, 101-105. https://doi.org/10.1016/j.catcom.2017.12.022

[4] Zhang, B., Hou, Y., Yu, Z., Liu, Y., Huang, J., Qian, L. and Xiong, J. (2019) Three-Dimensional Electro-Fenton Degradation of Rhodamine B with Efficient Fe-Cu/kaolin Particle Electrodes: Electrodes Optimization, Kinetics, Influencing Factors and Mechanism. *Separation and Purification Technology*, **210**, 60-68. https://doi.org/10.1016/j.seppur.2018.07.084

[5] Marco, J.F. and Escalona, N. (2016) Preparation and Characterization of Bimetallic Fe-Cu Allophane Nanoclays and their Activity in the Phenol Oxidation by Heterogeneous Electro-Fenton Reaction. *Microporous and Mesoporous Materials*, **225**, 303-311. https://doi.org/10.1016/j.micromeso.2016.01.013

[6] Ren, W., Tang, D., Huang, M., Sun, J. and Lv, K. (2018) Remarkable Improved Electro-Fenton Efficiency by Electric-Field-Induced Catalysis of CeO_2. *Journal of* Hazardous *Materials*, **350**, 88-97. https://doi.org/10.1016/j.jhazmat.2018.02.018

[7] Yuan, S., Fan, Y., Zhang, Y., Tong, M. and Liao, P. (2011) Pd-Catalytic *In-Situ* Generation of H2O2 from H2 and O2 Produced by Water Electrolysis for the Efficient Electro-Fenton Degradation of Rhodamine B. *Environmental Science and Technology*, **45**, 8514-8520. https://doi.org/10.1021/es2022939

[8] Pi, L., Cai, J., Xiong, L., Cui, J., Hua, H., Tang, D. and Mao, X. (2020) Generation of H_2O_2 by On-Site Activation of Molecular Dioxygen for Environmental Remediation Applications: A Review. *Chemical Engineering Journal*, **389**, Article ID: 123420. https://doi.org/10.1016/j.cej.2019.123420

[9] Luo, M., Yuan, S., Tong, M., Liao, P., Xie, W. and Xu, X. (2014) An Integrated Catalyst of Pd Supported on Magnetic Fe_3O_4 Nanoparticles: Simultaneous Production of H_2O_2 and Fe^{2+} for Efficient Electro-Fenton Degradation of Organic Contaminants. *Water Research*, **48**, 190-199. https://doi.org/10.1016/j.watres.2013.09.029

[10] Thokchom, B., Qiu, P., Cui, M., Park, B., Pandit, A.B. and Khim, J. (2017) Magnetic Pd@Fe_3O_4 Composite Nanostructure as Recoverable Catalyst for Sonoelectrohybrid Degradation of Ibuprofen. *Ultrasonics Sonochemistry*, **34**, 262-272. https://doi.org/10.1016/j.ultsonch.2016.05.030

[11] Xu, X., Liao, P., Yuan, S., Tong, M., Luo, M. and Xie, W. (2013) Cu-Catalytic Generation of Reactive Oxidizing Species from H_2 and O_2 Produced by Water Electrolysis for Electro-Fenton Degradation of Organic Contaminants. *Chemical Engineering Journal*, **233**, 117-123. https://doi.org/10.1016/j.cej.2013.08.046

[12] Jinisha, R., Gandhimathi, R., Ramesh, S.T., Nidheesh, P.V. and Velmathi, S. (2018) Removal of Rhodamine B Dye from Aqueous Solution by Electro-Fenton Process Using Iron-Doped Mesoporous Silica as a Heterogeneous Catalyst. *Chemosphere*, **200**, 446-454. https://doi.org/10.1016/j.chemosphere.2018.02.117

[13] Setayesh, S.R., Nazari, P. and Maghbool, R. (2020) Engineered $FeVO_4/CeO_2$ Nanocomposite as a Two-Way Superior Electro-Fenton Catalyst for Model and Real Wastewater Treatment. *Journal of Environmental Sciences*, **97**, 110-119. https://doi.org/10.1016/j.jes.2020.04.035

[14] Tian, P., Xu, X., Ao, C., Ding, D., Li, W., Si, R. and Tu, W. (2017) Direct and Selective Synthesis of Hydrogen Peroxide over Palladium-Tellurium Catalysts at Ambient Pressure. *ChemSusChem*, **10**, 3342-3346. https://doi.org/10.1002/cssc.201701238

[15] Wang, S., Gao, K., Li, W. and Zhang, J. (2017) Effect of Zn Addition on the Direct Synthesis of Hydrogen Peroxide over Supported Palladium Catalysts. *Applied Catalysis A*: *General*, **531**, 89-95. https://doi.org/10.1016/j.apcata.2016.10.023

[16] Li, J., Ishihara, T. and Yoshizawa, K. (2011) Theoretical Revisit of the Direct Synthesis of H_2O_2 on Pd and Au @ Pd Surfaces: A Comprehensive Mechanistic Study. *Journal of Physical Chemistry A*, **115**, 25359-25367. https://doi.org/10.1021/jp208118e

[17] Ding, D., Xu, X., Tian, P., Liu, X., Xu, J. and Fan, Y. (2018) Promotional Effects of Sb on Pd-Based Catalysts for the Direct Synthesis of Hydrogen Peroxide at Ambient Pressure. *Chinese Journal of Catalysis*, **39**, 673-681. https://doi.org/10.1016/S1872-2067(18)63031-1

[18] Maity, S. and Eswaramoorthy, M. (2016) Ni-Pd Bimetallic Catalysts for the Direct Synthesis of H_2O_2-Unusual Enhancement of Pd Activity in the Presence of Ni. *Journal of Materials Chemistry A*, **5**, 3233-3237. https://doi.org/10.1039/C6TA00486E

[19] Freakley, S.J., He, Q., Harrhy, J.H., Lu, L., Crole, D.A., Morgan, D.J., Ntainjua, E.N., Edwards, J.K., Carley, A.F., Borisevich, A.Y., Kiely, C.J. and Hutchings, G.J. (2016) Palladium-Tin Catalysts for the Direct Synthesis of H_2O_2 with High Selectivity. *Science*, **351**, 965-968. https://doi.org/10.1126/science.aad5705

[20] Edwards, J.K., Freakley, S.J., Carley, A.F., Kiely, C.J. and Hutchings, G.J. (2014) Strategies for Designing Supported Gold À Palladium Bimetallic Catalysts for the Direct Synthesis of Hydrogen Peroxide. *Accounts of Chemical Research*, **47**, 845-854. https://doi.org/10.1021/ar400177c

[21] Kresse, G. and Furthmiiller, J. (1996) Efficiency of *Ab-Initio* Total Energy Calculations for Metals and Semiconductors Using a Plane-Wave Basis Set. *Computational*

Materials Science, **6**, 15-50. https://doi.org/10.1016/0927-0256(96)00008-0

[22] Perdew, J.P., Burke, K. and Ernzerhof, M. (1996) Generalized Gradient Approximation Made Simple. *Physical Review Letters*, **77**, 3865-3868. https://doi.org/10.1103/PhysRevLett.77.3865

[23] Hendrik, J. and James, D. (1977) Special Points for Brillouin-Zone Integrations. *Physical Review B*, **16**, 1746-1747. https://doi.org/10.1103/PhysRevB.16.1746

[24] Henkelman, G. and Jónsson, H. (2000) Improved Tangent Estimate in the Nudged Elastic Band Method for Finding Minimum Energy Paths and Saddle Points. *The Journal of Chemical Physics*, **113**, 9978. https://doi.org/10.1063/1.1323224

[25] Lari, G.M., Puértolas, B., Shahrokhi, M., López, N. and Pérez-Ramírez, J. (2017) Hybrid Palladium Nanoparticles for Direct Hydrogen Peroxide Synthesis: The Key Role of the Ligand. *Angewandte Chemie*, **129**, 1801-1805. https://doi.org/10.1002/ange.201610552

[26] Yalfani, M.S., Contreras, S., Medina, F. and Sueiras, J.E. (2011) Hydrogen Substitutes for the *in Situ* Generation of H_2O_2: An Application in the Fenton Reaction. *Journal of Hazardous Materials*, **192**, 340-346. https://doi.org/10.1016/j.jhazmat.2011.05.029

[27] Blanco-Brieva, G., De FrutosEscrig, M.P., Campos-Martin, J.M. and Fierro, J.L.G. (2010) Direct Synthesis of Hydrogen Peroxide on Palladium Catalyst Supported on Sulfonic Acid-Functionalized Silica. *Green Chemistry*, **12**, 1163-1166. https://doi.org/10.1039/c003700a

[28] Kim, J.K., Lee, J.K., Kang, K.H., Lee, J.W. and Song, I.K. (2015) Catalytic Decomposition of Phenethyl Phenyl Ether to Aromatics over Pd-Fe Bimetallic Catalysts Supported on Ordered Mesoporous Carbon. *Journal of Molecular Catalysis A*: *Chemical*, **410**, 184-192. https://doi.org/10.1016/j.molcata.2015.09.023

[29] Liao, M., Hu, Q., Zheng, J., Li, Y., Zhou, H., Zhong, C. and Chen, B.H. (2013) Pd Decorated Fe/C Nanocatalyst for Formic Acid Electrooxidation. *Electrochimica Acta*, **111**, 504-509. https://doi.org/10.1016/j.electacta.2013.08.102

[30] Sellers, R.M. (1990) Spectrophotometric Determination of Hydrogen Peroxide Using Potassium Titanium (IV) Oxalate. *Analyst*, **105**, 950-954. https://doi.org/10.1039/an9800500950

[31] Singla, R., Ashokkumar, M. and Grieser, F. (2004) The Mechanism of the Sonochemical Degradation of Benzoic Acid in Aqueous Solutions. *Research on Chemical Intermediates*, **30**, 723-733. https://doi.org/10.1163/1568567041856963

[32] Song, X., Sun, K., Hao, X., Su, H., Ma, X. and Xu, Y. (2019) Facet-Dependent of Catalytic Selectivity: The Case of H2O2 Direct Synthesis on Pd Surfaces. *Journal of Physical Chemistry A*, **123**, 26324-26337. https://doi.org/10.1021/acs.jpcc.9b07097

[33] Ouyang, L., Da, G., Tian, P., Chen, T., Liang, G., Xu, J. and Han, Y. (2014) Insight into Active Sites of Pd-Au/TiO_2 Catalysts in Hydrogen Peroxide Synthesis Directly from H_2 and O_2. *Journal of Catalysis*, **311**, 129-136. https://doi.org/10.1016/j.jcat.2013.11.008

[34] Tian, P., Ding, D., Sun, Y., Xuan, F., Xu, X., Xu, J. and Han, Y. (2019) Theoretical Study of Size Effects on the Direct Synthesis of Hydrogen Peroxide over Palladium Catalysts. *Journal of Catalysis*, **369**, 95-104. https://doi.org/10.1016/j.jcat.2018.10.029

[35] Pengfei, T., Like, O., Xinchao, X.U., Jing, X.U. and Fan, H.A.N.Y. (2013) Density Functional Theory Study of Direct Synthesis of H_2O_2 from H_2 and O_2 on Pd(111), Pd(100), and Pd(110) Surfaces. *ChineseJournal of Catalysis*, **34**, 1002-1012.

https://doi.org/10.1016/S1872-2067(12)60537-3

[36] Nidheesh, P. V., Gandhimathi, R., Velmathi, S. and Sanjini, N.S. (2014) Magnetite as a Heterogeneous Electro Fenton Catalyst for the Removal of Rhodamine B from Aqueous Solution. *RSC Advances*, **4**, 5698-5708. https://doi.org/10.1039/c3ra46969g